ADVANCED MATERIALS

DOI: 10.1002/adma.200602262

Weaving Genetically Engineered Functionality into Mechanically Robust Virus Fibers**

By *Chung-Yi Chiang*, *Charlene M. Mello*,* *Jiji Gu*, *Emilio C. C. M. Silva*, *Krystyn J. Van Vliet*,* and *Angela M. Belcher**

Despite the increasing need for material multifunctionality in optical and semiconducting fibers, antimicrobial textiles, molecular-filtration membranes, and other applications, the production of functionalized fibers has posed a challenge in materials science and engineering. Here we report the design and synthesis of fibers with genetically controllable and functionalized surfaces using M13 filamentous viruses (or bacteriophages). This work applies genetic engineering, chemical conjugation, and biotemplating methods to produce continuous fibers of centimeter-scale length and micrometer-scale diameter from nanometer-scale virus scaffolds. In addition, we find the virus fibers to be mechanically comparable to synthetic homopolymer fibers. The tunable functionalities and mechanical properties of the virus fibers show the promise of these high-aspect-ratio structures as useful materials for various applications including detection, catalysis, energy storage, and power generation.

Increasing demand for tuning the molecular dimensions, structures, and functionalities in nanoscience has driven the search for materials with precisely controllable properties. Fibers are currently used in energy and electronic applications to obtain high energy density, energy capacity, and transportation efficiency, which may all be further improved by using nanostructured materials.[1–4] Synthetic polymers are commonly used as fiber materials;[5,6] however, as it is difficult to produce varied functionalities on a single-fiber surface, synthetic polymer-based fibers often lack functional versatility. Surface modifications of synthetic fibers usually require multistep chemical modifications and/or expensive enzyme treatments.[6–9] In addition, because of the lack of control over molecular structures and conformations, mixing incompatible functionalities in a material often leads to disorganized structures at the molecular level or to micro- to macroscopic phase separation, resulting in unintended or defective functionalities in the fiber surface.

Consequently, biological macromolecules such as DNA, proteins, and micro-organisms (e.g., virus and fungi) have become key material-design components because of the inherent nanoscale control of molecular functionalities and structures.[10–14] In nature, functionalities and hierarchical structures of fibrous proteins are precisely controlled by DNA and widely used to construct strong and functional fibers such as spider silk[15–17] and collagen.[18] However, these natural proteins are already highly evolved for specific functions, and it is difficult to engineer new design parameters into them. By adopting and combining the principles of fabrication found both in nature and in laboratories, we can design the building blocks with desired functionality and structural hierarchy at the nanometer level and further assemble these building blocks into continuous, mechanically robust fibers.

Here we employ the M13 filamentous virus as a genetically controlled organic building block. M13 bacteriophage has a high aspect ratio with a length of about 880 nm and a diameter of 6–7 nm. Its hierarchical structure and functionalities are genetically controlled by the single-stranded viral DNA packed within the bacteriophage. The virus displays about 2700 copies of pVIII major coat proteins along its longitudinal axis, with functionalities that can be altered via modification of the viral genome. For example, the virus can be modified to display peptides, which are capable of binding, nucleating, and organizing specific inorganic materials.[19–22] To select a suitable peptide for mediating a specific material interaction with a virus template, an evolutionary screening process called biopanning is commonly used. This technique has been used to identify peptides that assist to produce metallic (e.g., Au) and semiconducting (e.g., ZnS) virus-based nanoarchitectures including nanowires and nanoparticle arrays.[19,23,24] Additionally, M13 contains various chemical functional groups, which can be genetically programmed to be expressed on the pVIII proteins of the virus and are chemically accessible to a variety of reagents.[25] Thus, an M13 virus can be chemically and genetically modified to obtain desired functionalities.

[*] Prof. K. J. Van Vliet, E. C. C. M. Silva
Department of Materials Science and Engineering
Department of Civil and Environmental Engineering
Massachusetts Institute of Technology
8-237, 77 Massachusetts Ave., Cambridge, MA 02139 (USA)
E-mail: krystyn@mit.edu
Prof. A. M. Belcher, C.-Y. Chiang, J. Gu
Department of Materials Science and Engineering
Division of Biological Engineering
Massachusetts Institute of Technology
16-244, 77 Massachusetts Ave., Cambridge, MA 02139 (USA)
E-mail: belcher@mit.edu
Dr. C. M. Mello
Macromolecular Science Team, U.S. Army Research
Development and Engineering Command, Natick Solider Center
Kansas St., Natick, MA 01760 (USA)
E-mail: Charlene.Mello@us.army.mil

[**] This work was supported by the Army Research Office Institute of Collaborative Biotechnologies, and the David and Lucile Packard Foundation. Supporting Information is available online from Wiley InterScience or from the author.

The ease of modifying M13 makes this virus an attractive platform for the growth and assembly of a variety of materials. At sufficiently high concentrations, M13 viruses behave as lyotropic liquid-crystalline mesogens and self-organize to form micrometer-scale long-range order in aqueous solutions.[26,27] The liquid-crystalline property of M13 is driven by its high aspect ratio and anisotropic polarity. Inspired by the synthesis routes and properties of natural fibers,[28] we used viral liquid-crystalline solutions to fabricate virus-based fibers.[29] Here, our goal was to fabricate genetically functionalized fibers by spinning engineered M13 viruses. We demonstrate two routes to fabricate two different virus-based functional fibers: i) biotemplating the viruses with desired functionality before spinning the viruses into fibers; and ii) spinning evolutionally selected and genetically modified viruses into fibers or outer sheaths of fibers for subsequent biotemplating.

For the former case, we chemically conjugated amine-terminated cadmium selenide quantum dots (QDs) to M13 virus templates via the carboxylic acid side groups displayed on the pVIII proteins. A continuous fiber of micrometer-scale diameter (microfiber) was created through a wet-spinning process where a concentrated QD-conjugated virus solution was spun vertically into 2.5 % glutaraldehyde solution at a constant rate (see Experimental). The virus fibers containing QDs emit red light under exposure to UV light (Fig. 1a and b). This demonstrates that conjugated QDs can be retained in virus fibers after the wet-spinning and washing processes. These QD/fiber assemblies may serve as optical devices and advanced sensors.[30] To adjust the optical performance of a virus fiber, increasing the displayed copies of carboxylic acid side groups on pVIII proteins may result in relatively higher quantity of QDs to be conjugated to the virus. To demonstrate this surface tunability, a genetically engineered glutamate (Glu)-rich virus, named E4, was used for QD conjugation. This virus contains four Glus and one aspartate (Asp) in the outer six amino acids at the N-terminus of the pVIII protein. Compared with the wild-type M13KE virus (New England Biolabs, Inc), E4 has two additional Glus in the outer part of each pVIII protein and therefore exhibits increased conjugation of amine-terminated QDs (Fig. 1c). This experiment demonstrates that genetic engineering is essential to improve or tune the biotemplating properties.

For the latter fabrication route, we demonstrated the capability of surface-functionalized M13 virus to construct self-supported or composite functional fibers for subsequent bio-

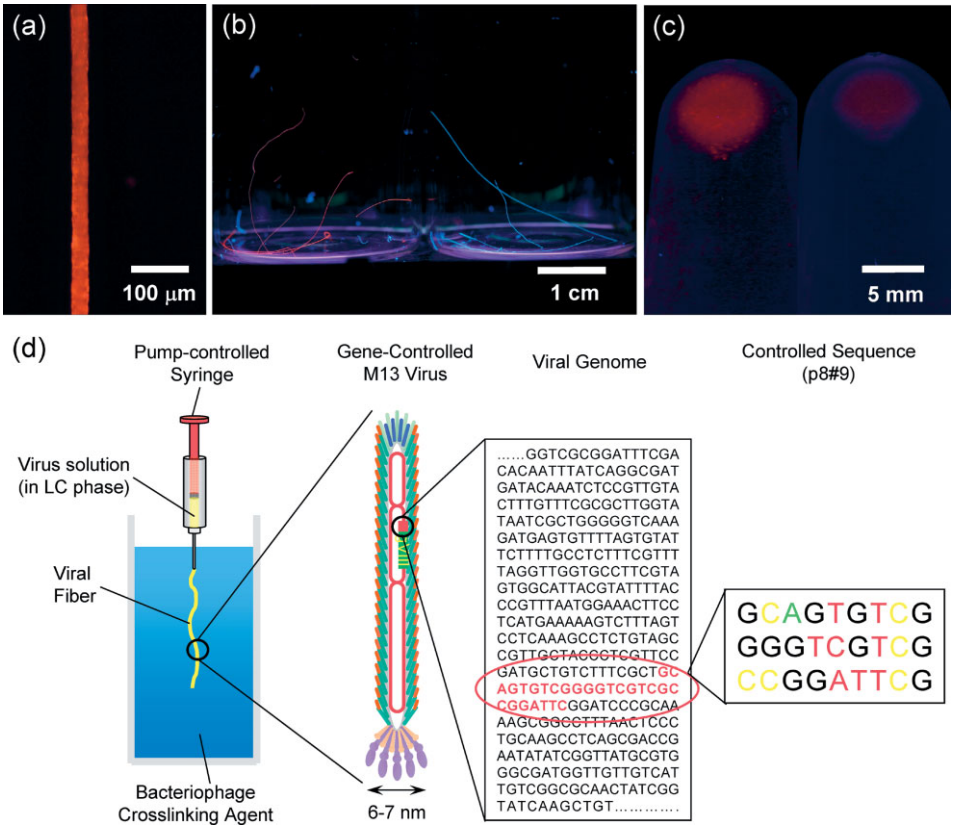

Figure 1. Images and schematic design of chemically and genetically engineered functional fibers. a) Fluorescence microscopy image of E4 virus (a genetically engineered glutamate (Glu)-rich virus) fiber conjugated with QDs excited by using UV light. b) Under exposure to UV light, virus fibers conjugated with QDs emit red light (left) and nonconjugated virus fibers emit blue light (right). c) The E4 virus (left) shows a relatively higher intensity of light emission than the wild-type M13KE virus (right) after QD conjugation and purification. d) Schematic illustration of an inserted DNA sequence displaying specific peptides (orange) along the M13 virus that is spun into a fiber with the desired surface functionality.

ADVANCED MATERIALS

templating of gold. The peptide sequence Valine–Serine–Glycine–Serine–Serine–Proline–Aspartate–Serine (Val–Ser–Gly–Ser–Ser–Pro–Asp–Ser), termed p8#9, was selected from screening a type 8 bacteriophage library on gold substrates. Genetically modified M13 virus containing p8#9 peptides has been shown previously to act as a template for growing gold nanowires and gold nanoparticle arrays.[23] Through genetic engineering, bacteriophage building blocks provide flexibility in designing and modifying the fiber surface (Fig. 1d).

Continuous microfibers were produced using the same wet-spinning process described above. After the virus fibers were rinsed with water to remove unreacted glutaraldehyde, gold nanoparticles were directly nucleated from aqueous Au^{3+} solutions upon reduction with $NaBH_4$, resulting in nanoparticles which bound specifically to the engineered virus fibers at room temperature. The fiber surface and the distribution of biotemplated gold on the virus fibers were analyzed using scanning electron microscopy (SEM) and energy-dispersive X-ray (EDX) imaging. The homogeneous coating of gold nanoparticles on the genetically functionalized p8#9 fibers indicates the correct presentation of functionalities on the virus fiber surface (Fig. 2a).

To demonstrate the specificity of this gold-binding ability on genetically engineered M13 virus fibers, fibers were also spun from a wild-type clone, M13KE, which does not contain the gold-binding functionality. These control fibers contained discrete and scattered gold islands on the fiber surfaces after the identical processing for the p8#9 fibers (Fig. 2b). Although the surface roughness of virus fibers provides high surface tension, which may be expected to facilitate nonspecific binding of gold particles onto the fiber, the M13KE fiber itself still exhibited low gold-binding affinity. The low affinity resulted in a low density of gold on the M13KE fiber surface.

The ability of Kevlar fibers to bind gold was also explored. These synthetic homopolymer fibers showed a negligible amount of gold deposition (Fig. 2c). Absence of binding affinity to gold and the smooth surface of these synthetic fibers resulted in poor adhesion of gold particles. To create multifunctional fibers having high mechanical strength and capability of surface mineralization, a core/sheath structure was achieved, using Kevlar as the core material and the engineered virus as the sheath. A Kevlar fiber was dipped into a minimally crosslinked gold-binding virus suspension containing 0.05 % glutaraldehyde. Both Kevlar and the virus contain functional groups in their chemical structures that contribute to secondary forces, such as hydrogen-bonding and hydrophobic interactions, resulting in adhesion between Kevlar and the virus. This virus-coated Kevlar fiber was then transferred to a 2.5 % glutaraldehyde solution to continue the crosslinking reaction. After coating with this gold-binding virus, gold nanoparticles were templated directly onto the composite fiber (Fig. 2d).

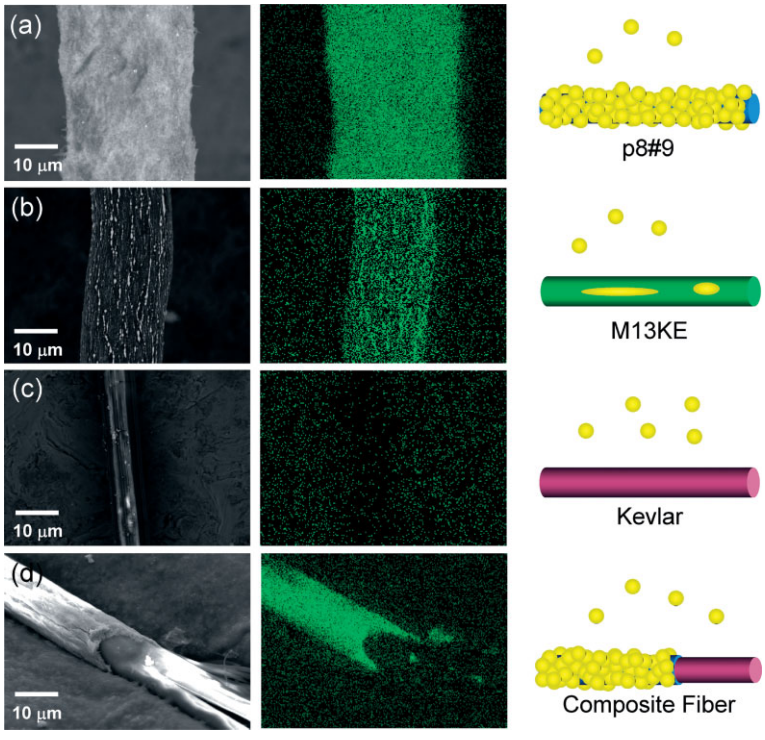

Figure 2. Effects of genetic engineering on mineralization. SEM and EDX images, and schematic representations of different types of fibers after gold mineralization. a) Dense gold nanoparticles are homogeneously mineralized on a fiber comprising viruses (p8#9) selected to bind gold nanoparticles. b) The M13KE fiber contains no specific gold-binding affinity and exhibits a small amount of random binding to gold particles. c) The Kevlar fiber exhibits limited, if any, gold-particle attachment. d) Nucleation of gold nanoparticles is only observed on the portion of a Kevlar fiber coated with p8#9 viruses.

Although agents such as glutaraldehyde will crosslink the amine groups at the N-termini of pVIII proteins, no disruption of surface functionality of the M13 viruses in these fibers was observed. This demonstrates the capability of the genetically engineered nanometer-scale virus scaffold to mineralize inorganic materials at ambient temperature and to retain the desired functionality when assembled as microfibers. Such micrometer-sized fibers containing nanoparticles may be used in catalytic filtration, battery electrodes, and photovoltaic devices.[1,20,31]

The reproducible dimensions and structures of these centimeter-long fibers enabled us to study the mechanical properties of virus fibers for the first time. Although reports discussing the mechanics of protein-based natural fibers have been reported,[32,33] the mechanical properties of virus-based fibers have not yet been considered. To evaluate the practical applications of such functional fibers, the elastic modulus, yield and ultimate tensile strength, failure stress and strain, and strain-rate sensitivity of the virus fibers were measured. To verify the effects of the virus crosslinking density on the fiber mechanical properties, virus fibers were synthesized in various concentrations of glutaraldehyde ranging from 0 % to 10 % (v/v). The estimated spinning rate was 5.3 cm min^{-1} for all

concentrations tested. A change in the liquid-crystalline phase during fiber spinning is expected to directly affect the mechanical properties of the virus fibers because of the orientation of the viral particles. Thus, all the virus fibers were spun from nematic liquid-crystalline solutions to avoid variation resulting from different liquid-crystalline phases.

No fiber was formed in the absence of a crosslinking agent; the fibers spun into 0.1 % and 0.5 % glutaraldehyde were diffuse and semitransparent; and the fibers spun into a crosslinking agent of ≥1 % were solid and opaque. The diameters of the fibers varied from 10 to 50 μm depending on the spinning rate, the percentage of glutaraldehyde, and effective strain ($(L_f - L_i)/L_i$, where L_i is the initial length of fiber spun from the spinneret in the wet state and L_f is the final length of fiber in the dry state). All the fibers could be pulled out of the solution by using forceps, indicating sufficient strength for mechanical processing such as drawing and weaving.

Uniaxial tensile tests were conducted to examine the mechanical properties of these virus fibers in the dry state (Fig. 3a). On average, engineering stress–strain responses of pure virus fibers indicated a Young's elastic modulus E of ca. 3 GPa, an ultimate tensile strength σ_u of ca. 33 MPa, and an ultimate tensile strain ε_u of ca. 1.3 %. Overall, E of the pure-virus fiber was similar to that of Nylon 6,6 (E = 1–3 GPa) and glassy homopolymers such as polystyrene (E = 2–4 GPa). Fiber ultimate tensile strength σ_u was comparable to that of atactic polystyrene and polytetrafluorethylene (σ_u = 15–50 MPa).[34] The normalized tensile strength (σ_u/E) of the virus fibers (0.005–0.030) was bounded by that of Nylon 6,6 (0.02–0.06) and polystyrene (0.002–0.02),[35] indicating that the mechanical strength of virus fiber is similar to common synthetic (and glassy) homopolymers (see Supporting Information).

Mechanical data were analyzed statistically using one-way ANOVA (analysis of variance). When varying the crosslinker concentrations in the processing, statistically significant changes occurred in stiffness as quantified by E ($F(4,20) = 2.919$; $F(x,y)$ is the measurement of difference between individual distributions, where x is the degrees of freedom for the between group, and y is the degress of freedom for the within group, probability $p < 0.047$) (Fig. 3b) and effective ductility as quantified by ε_u ($F(4,20) = 4.966$, $p < 0.006$); however, changes in strength as quantified by σ_u as a function of the percentage of glutaraldehyde were not statis-

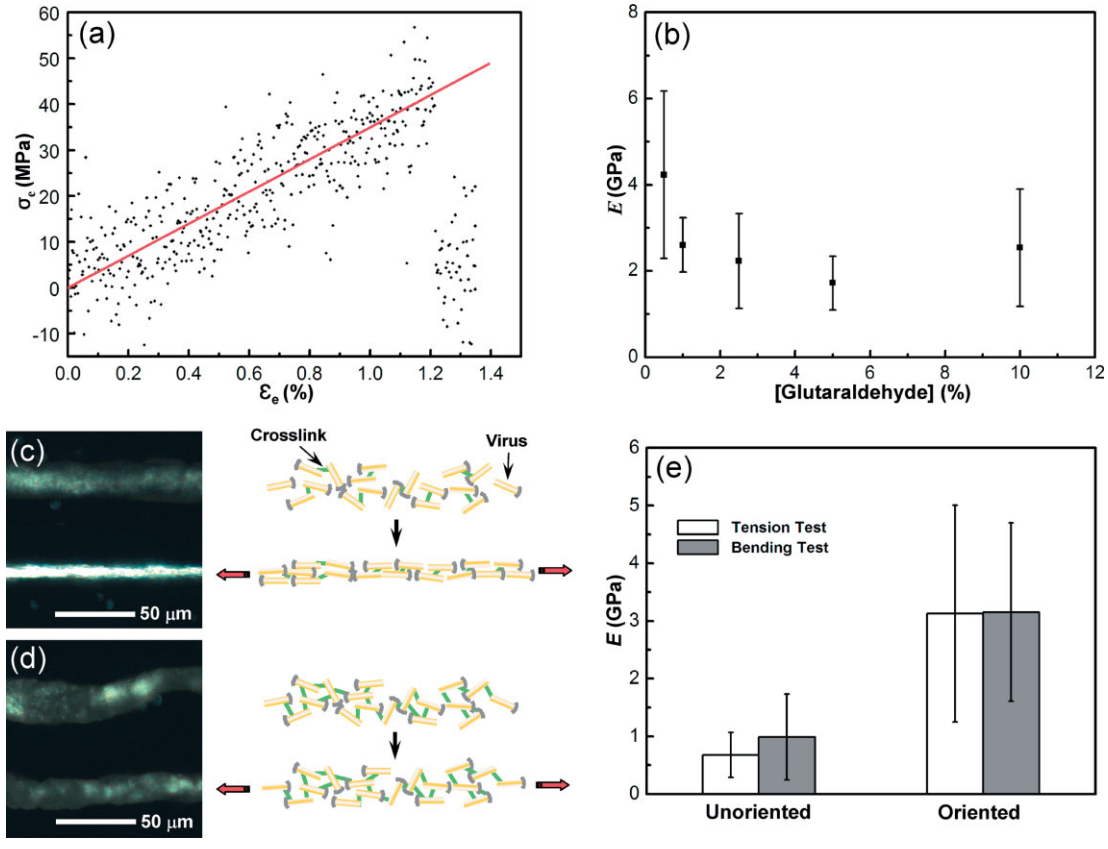

Figure 3. Mechanical properties of virus fibers. a) Representative engineering stress–strain response of virus fibers. No plastic deformation is observed until fiber fracture. b) Effects of glutaraldehyde concentration on the Young's modulus E shows a local minimum around 5 % glutaraldehyde. c,d) Polarized optical microscopy (POM) images of virus fibers (left) and schematic graphs of virus assemblies (right), where rods represent individual virus particles constrained by crosslinks (green). The virus fibers fabricated from 0.5 % (c) and 5 % (d) glutaraldehyde solutions before stretching (top) and after manual elongation while drying (bottom). e) Comparison of E for unoriented and oriented virus fibers consisting of 0.5 % glutaraldehyde solution under uniaxial tension test and cantilevered bending test.

ADVANCED MATERIALS

tically significant ($F(4,20) = 0.9765, p < 0.44$) (Supporting Information). It is important to note that the variation of measured mechanical properties is attributed to both the resolution of the uniaxial tensile apparatus and the imprecise elongation of virus fibers during the drying process, the latter of which affects the extent of fiber crystallinity, as discussed below.

The extent of elongation in the wet state and the crosslinking density of a virus fiber will determine the percentage of crystallinity in the fiber and its mechanical properties. Virus fibers fabricated from < 1 % glutaraldehyde can be elongated 5–20 % before drying in air. The maximum E was observed for the lowest crosslinker concentration of 0.5 % glutaraldehyde. This is because the crosslinking density of the virus fiber determines the degrees of freedom of virus orientation during the processing prior to drying. The effects of virus orientation on fiber crystallinity were observed using polarized optical microscopy (POM) (Fig. 3c and d). The crystallinity of the virus fibers with low crosslinking density can be easily increased by elongating the wet fibers. This elongation process reorients the virus particles and promotes secondary interactions among viruses. In other words, low crosslinking density gives the fibers sufficiently high degrees of freedom for reorientation of the virus particles upon extension in the wet state. Conversely, for the fibers with high crosslinking density, the virus particles have limited degrees of freedom, resulting in a lower degree of crystallinity even upon elongation of the virus fiber in the wet state.

An independent set of samples was tested under uniaxial tension and bending to examine the effects of virus orientation on fiber mechanical properties (Fig. 3e). In this experiment, oriented fibers were elongated at least 15 % in the wet state and analyzed to measure E in the dry state. Under uniaxial tension, we observed that the stiffness E of the oriented virus fiber (3.13 ± 1.88 GPa) increased significantly compared to the unoriented fiber (0.68 ± 0.39 GPa) and that the strength σ_u of the oriented fiber (35.05 ± 25.53 MPa) also increased significantly with respect to the unoriented counterpart (6.02 ± 5.40 MPa). The bending stiffness (force P normalized by free-end displacement d) of the same set of samples was also measured using scanning probe microscopy (SPM)[36,37] at different force application points ($x + x'$) along the cantilevered virus fiber (see Experimental and Supporting Information). The elastic moduli E acquired via this method were (0.98 ± 0.74) GPa and (3.15 ± 1.54) GPa for nonoriented and oriented virus fibers, respectively, which agreed well with that measured via uniaxial tension. We therefore conclude that the crosslinker is only needed to process the virus fibers via spinning but is not necessary to enhance the mechanical properties of virus fibers. In the case of virus fibers with low chemical crosslinking densities, both the mechanical strength and stiffness is attributable to secondary interviral interactions such as hydrogen-bonding and ionic interactions, and the mechanical properties can be enhanced through fiber elongation that promotes crystallinity via environmentally benign processing.

To evaluate the extent of viscoelasticity in the virus fibers, uniaxial tensile tests were conducted at three different displacement rates: 10^{-2}, 10^{-3}, and 10^{-4} mm s^{-1}, corresponding to strain rates $\dot{\varepsilon}_H$ of 10^{-1} to 10^{-3} s^{-1} (see Supporting Information). A slight increase in E ($F(2,12) = 4.974$, $P < 0.027$) and decrease in ε_u ($F(2,12) = 27.78$, $P < 0.0001$) were observed as a function of $\dot{\varepsilon}_H$. For a 100-fold increase in strain rate, E increased only by 1.5-fold. This indicates that the virus fibers are well approximated as linearly elastic materials, and do not exhibit sufficient viscous damping over these strain rates. In addition, no statistically significant change in σ_u ($F(2,12) = 0.8042$, $P < 0.47$) was observed over this strain-rate range. Neither necking nor significant plastic deformation prior to fracture was observed under uniaxial tension (Fig. 3a), and the fracture surfaces appeared globally brittle (flat and normal to the loading axis) under optical microscopy (see Supporting Information). However, SEM images showed locally ductile fracture features (< 1 μm in length and < 20 nm in width) across the whole fracture surface of the virus fiber (see Supporting Information). The fracture surface was perpendicular to the loading axis and was microscopically rough because of this localized pull-out of virus material. Thus, the mechanical failure of these virus fibers appears macroscopically brittle and microscopically ductile, consistent with the hydrostatic stress-sensitive failure surface of brittle polymers.[38]

After nucleation of gold nanoparticles on the virus fibers, E decreased to 0.2–1.5 GPa, due most likely to the chemical and physical deterioration caused by the reducing agent and the formation of gold inside the fibers. This deterioration may be avoided by employing a milder reduction reaction for gold, such as hydrogen reduction. On the other hand, the composite fiber with a core-sheath structure maintained structural integrity upon gold nucleation: E of Kevlar fibers before virus functionalization was ca. 35 GPa, and remained unchanged after gold was mineralized onto the composite fibers (ca. 33 GPa). This indicates that viruses can serve as a functional template to alter the functionality of Kevlar fibers without any chemical or mechanical deterioration of the overall fiber mechanical properties.

This work provides a new conceptual scheme for fiber design and fabrication through genetic modification of a biotemplate. Using an engineered virus to continuously produce functional materials or coatings for synthetic fibers could simplify current surface-modification processes such as multistep chemical or enzymatic treatments. We demonstrate the potential of the M13 virus to serve as a powerful toolkit for designing a specific functional fiber material from standard techniques including biopanning, bacteriophage amplification, and genome modification. The virus fibers exhibit mechanical toughness and strength comparable to synthetic polymer fibers, indicating that this filamentous virus can be integrated into current fibril and woven-mesh manufacturing systems. The genetic manipulation of diverse functionalities on the virus fiber surfaces offers a convenient and powerful basis for conjugating organic or inorganic materials for a variety of applications such as the creation of antimicrobial, catalytic, optical, medical, and electronic materials.

Experimental

Chemical Conjugation of Quantum Dots to the M13 Virus: To conjugate QDs to M13 viruses, 5 μL 1-ethyl-3-(3dimethylaminopropyl)-carbodiimide hydrochloride (EDC, ~200 mM) was added to 200 μL virus solution (ca. 5.5×10^{11} plaque-forming units (pfu) μL^{-1} in Milli-Q water), which was mixed with 5 μL QD solution (8.25 μM, Qdot 705 ITK amino QDs, Invitrogen Corp.). The mixture was vortexed and incubated at room temperature for 1.5 h. After adding 40 μL polyethylene glycol (PEG)/NaCl solution (20 % (w/v) polyethylene glycol-8000, 2.5 M NaCl), the mixture was centrifuged at 10 000 rpm for 10 min. Unbound QDs in the supernatant were removed, and the virus pellet was resuspended in 10 μL Milli-Q water.

Fiber Preparation and Gold Mineralization: A concentrated virus solution (ca. 470 mg mL^{-1} in Milli-Q water, 1.7×10^{13} pfu μL^{-1}) was spun vertically through a 33 gauge needle into a glutaraldehyde solution by a syringe pump at a constant speed of 0.025 mL h^{-1}, producing approximately 13 cm of virus fiber per microliter of viral suspension. After incubating in glutaraldehyde for 2 h, virus fibers were rinsed with Milli-Q water. These fibers were then vertically pulled out of the water by using forceps and dried in air. To test the gold-mineralization capability of fibers, the wet fiber was immersed in a 300 μL chloroauric acid solution (5 mM, pH 7.5) and incubated on ice for 10 min. A 150 μL sample of ice-cold sodium borohydride solution (5 mM) was then added to reduce the gold. After 12 h, the fiber was manually removed from the solution, rinsed with Milli-Q water, and dried in air.

Microscopy and Energy Dispersive X-ray Characterization: POM and fluorescence microscopy images were obtained using an optical microscope (Olympus IX51). SEM images were analyzed with FEI/Philips XL30 Field-Emission Gun Environmental Scanning Electron Microscope, operated at 10 kV with an electron-backscattering detector. EDX images were collected at a resolution of 256×200 pixels with 256 frames.

Uniaxial Tensile Testing: Under dry conditions, the ends of each fiber were secured between two stainless steel shims coated with cyanoacrylate, and the uniaxial tension tests were performed using 8848 Micro Tester (Instron Corp.) at ambient temperature, humidity, and pressure. Strain was recorded as crosshead displacement measured by using a digital optical encoder within the load train.

Bending Stiffness: The fibers were mounted as end-clamped cantilevers and fixed at one end with cyanoacrylate at the edges of glass slides. A scanning probe microscope (3D-Molecular Force Probe, Asylum Research) was used to acquire the force-displacement response of the fibers via deflection of silicon nitride cantilevers (OMCL-AC160TS, Olympus Corp.). The optical-lever sensitivity of the silicon nitride cantilevers was 41.64–47.35 nm V^{-1} and the spring constant k, calculated from the thermal vibration spectrum, was 59.25–71.36 N m^{-1}. Bending stiffness measured at different force application points can be interpreted to obtain E of the virus fiber and x' using the nonlinear relation:

$$\frac{P}{d} = \frac{3EI}{(x + x')^3} \quad (1)$$

where I is the moment of inertia of the cylindrical fibers. In Equation 1, d is the free-end displacement of a cantilevered fiber when it is subjected to a force P, x is the distance from the application point to the reference point, x' is the distance from the reference point to the support, and the moment of inertia I equals $\pi D^4/64$ for a cylindrical fiber of diameter D.

Error Analysis: The dimensions of the fiber and the resolution of the uniaxial tensile apparatus were the dominant sources of error in the mechanical properties measured here. The resolution of the uniaxial tensile apparatus is 0.1 μm in displacement and 10 nN in force. The suspended length of the fiber was measured using a digital caliper with an error of 0.1 %, and the fiber diameter was measured using optical microscopy with an error of 5 %. For SPM bending experiments, the SPM system calibration had 3 % error for both optical lever sensitivity and cantilever spring constant k. The linear fit of the uniaxial stress–strain response with an error of 1 % and the nonlinear fit of the SPM stiffness-position response with an error of 3 % were calculated using Microcal Origin. For each experimental variable, five specimens were tested via uniaxial tension or via cantilevered bending tests.

Received: October 4, 2006
Revised: November 1, 2006
Published online: February 19, 2007

[1] Y. X. Gu, D. R. Chen, M. L. Jiao, *J. Phys. Chem. B* **2005**, *109*, 17 901.
[2] R. Gvishi, U. Narang, G. Ruland, D. N. Kumar, P. N. Prasad, *Appl. Organomet. Chem.* **1997**, *11*, 107.
[3] M. S. Dresselhaus, G. Dresselhaus, *J. Electroceram.* **1997**, *1*, 273.
[4] L. F. Nazar, G. Goward, F. Leroux, M. Duncan, H. Huang, T. Kerr, J. Gaubicher, *Int. J. Inorg. Mater.* **2001**, *3*, 191.
[5] D. Li, Y. N. Xia, *Adv. Mater.* **2004**, *16*, 1151.
[6] M. L. Ma, Y. Mao, M. Gupta, K. K. Gleason, G. C. Rutledge, *Macromolecules* **2005**, *38*, 9742.
[7] Q. F. Wei, R. R. Mather, X. Q. Wang, A. F. Fotheringham, *J. Mater. Sci.* **2005**, *40*, 5387.
[8] G. M. Gubitz, A. C. Paulo, *Curr. Opin. Biotechnol.* **2003**, *14*, 577.
[9] J. M. Deitzel, W. Kosik, S. H. McKnight, N. C. B. Tan, J. M. DeSimone, S. Crette, *Polymer* **2002**, *43*, 1025.
[10] P. W. K. Rothemund, *Nature* **2006**, *440*, 297.
[11] J. D. Hartgerink, E. Beniash, S. I. Stupp, *Science* **2001**, *294*, 1684.
[12] C. E. Flynn, S. W. Lee, B. R. Peelle, A. M. Belcher, *Acta Mater.* **2003**, *51*, 5867.
[13] Z. Li, S. W. Chung, J. M. Nam, D. S. Ginger, C. A. Mirkin, *Angew. Chem. Int. Ed.* **2003**, *42*, 2306.
[14] R. L. Brutchey, E. S. Yoo, D. E. Morse, *J. Am. Chem. Soc.* **2006**, *128*, 10 288.
[15] P. A. Guerette, D. G. Ginzinger, B. H. F. Weber, J. M. Gosline, *Science* **1996**, *272*, 112.
[16] A. Lazaris, S. Arcidiacono, Y. Huang, J. F. Zhou, F. Duguay, N. Chretien, E. A. Welsh, J. W. Soares, C. N. Karatzas, *Science* **2002**, *295*, 472
[17] S. Sofia, M. B. McCarthy, G. Gronowicz, D. L. Kaplan, *J. Biomed. Mater. Res.* **2001**, *54*, 139.
[18] G. E. Fantner, T. Hassenkam, J. H. Kindt, J. C. Weaver, H. Birkedal, L. Pechenik, J. A. Cutroni, G. A. G. Cidade, G. D. Stucky, D. E. Morse, P. K. Hansma, *Nat. Mater.* **2005**, *4*, 612.
[19] C. Mao, D. J. Solis, B. D. Reiss, S. T. Kottmann, R. Y. Sweeney, A. Hayhurst, G. Georgiou, B. Iverson, A. M. Belcher, *Science* **2004**, *303*, 213.
[20] K. T. Nam, D. W. Kim, P. J. Yoo, C. Y. Chiang, N. Meethong, P. T. Hammond, Y. M. Chiang, A. M. Belcher, *Science* **2006**, *312*, 885.
[21] C. E. Fowler, W. Shenton, G. Stubbs, S. Mann, *Adv. Mater.* **2001**, *13*, 1266.
[22] W. Shenton, T. Douglas, M. Young, G. Stubbs, S. Mann, *Adv. Mater.* **1999**, *11*, 253.
[23] Y. Huang, C. Y. Chiang, S. K. Lee, Y. Gao, E. L. Hu, J. De Yoreo, A. M. Belcher, *Nano Lett.* **2005**, *5*, 1429.
[24] B. D. Reiss, C. B. Mao, D. J. Solis, K. S. Ryan, T. Thomson, A. M. Belcher, *Nano Lett.* **2004**, *4*, 1127.
[25] T. L. Schlick, Z. B. Ding, E. W. Kovacs, M. B. Francis, *J. Am. Chem. Soc.* **2005**, *127*, 3718.
[26] Z. Dogic, S. Fraden, *Phys. Rev. Lett.* **1997**, *78*, 2417.
[27] S. W. Lee, S. K. Lee, A. M. Belcher, *Adv. Mater.* **2003**, *15*, 689.
[28] K. Kerkam, C. Viney, D. Kaplan, S. Lombardi, *Nature* **1991**, *349*, 596.
[29] S. W. Lee, A. M. Belcher, *Nano Lett.* **2004**, *4*, 387.
[30] K. E. Meissner, C. Holton, W. B. Spillman, *Phys. E* **2005**, *26*, 377.
[31] M. Kemell, V. Pore, M. Ritala, M. Leskela, M. Linden, *J. Am. Chem. Soc.* **2005**, *127*, 14 178.

[32] G. H. Altman, F. Diaz, C. Jakuba, T. Calabro, R. L. Horan, J. S. Chen, H. Lu, J. Richmond, D. L. Kaplan, *Biomaterials* **2003**, *24*, 401.
[33] M. Feughelman, *J. Appl. Polym. Sci.* **2002**, *83*, 489.
[34] R. W. Hertzberg, in *Deformation and Fracture Mechanics of Engineering Materials*, Wiley, New York **1996**.
[35] C. A. Harper, *Handbook of Plastics, Elastomers & Composites*, McGraw-Hill, New York **2002**
[36] E. C. C. M. Silva, L. M. Tong, S. Yip, K. J. Van Vliet, *Small* **2006**, *2*, 239.
[37] M. Stolz, R. Raiteri, A. U. Daniels, M. R. VanLandingham, W. Baschong, U. Aebi, *Biophys. J.* **2004**, *86*, 3269.
[38] R. J. Young, P. A. Lovell, *Introduction to Polymers*, Chapman and Hall, New York **1991**.

